CHAPTER 6

EXPERIMENTAL SYNTHESIS, METHODS, AND RESULTS

OXIDATIVE DEHYDROGENATION OF ETHANE OVER REDUCED HETEROPOLYANION CATALYSTS

6.1 Experimental synthesis and methods

6.1.1 $M_xPMo_{12}Pyr$ (M = Nb, Mo, V)

Niobium and pyridine exchanged phosphomolybdic acids were prepared according to the methods presented by Holles et al.[1] and modified by Wight[2]. Exchange with molybdenum was performed according to Holles et al.[1] Phosphomolybdic acid ($H_3PMo_{12}O_{40}$) was obtained from Aldrich and used without further purification. Exchange with vanadium was accomplished by substitution of a vanadyl oxalate (GFS Chemicals) solution (0.06 g vanadyl oxalate/g water) for niobium oxalate in the above procedures. Synthesized materials are abbreviated $M_xPMo_{12}Pyr$, where M is the exchange metal and x denotes the ratio of the metal M to phosphorous (Keggin unit). The material $Nb_{0.6}PMo_{12}Pyr$ denotes niobium and pyridine exchanged $H_3PMo_{12}O_{40}$ with Nb/P = 0.6.

6.1.2 $Nb_xPMo_{11}VPyr$

Phospho—vanado—molybdic acid ($H_4PMo_{11}VO_{40}$) was either obtained from Pred Materials or synthesized according to Tsigdinos.[3] Niobium pentachloride, 5.003 g (Alfa Aesar, 99.999% packed under argon) was loaded into a three neck round bottom flask in a nitrogen atmosphere glove box and transferred to a Schlenck line. Water, 41.3 mL, was added dropwise via addition funnel with stirring. Hydrogen chloride vapors were neutralized with a sodium hydroxide bubbler. The solution was basified (pH = 12) by dropwise addition of 12.5 mL ammonium hydroxide (J. T. Baker, 28.0% – 30.0%). The white precipitate was dried by aspiration overnight and dissolved into a prepared solution of 4.60 g oxalic acid (Aldrich, 99+%) in 86.96 g water until complete dissolution of the precipitate.

Aliquots of the clear niobium oxalate solution were added dropwise to solutions of 1 g $PMo_{11}V$/1.5 g water and stirred for two hours at room temperature. The solutions were then heated with stirring to 80°C until all water evaporated. The resulting green solids were pulverized and slurried in water (1 g solid/6 g water). A seven-fold molar excess pyridine solution (0.1 g pyridine/1 g water) was added dropwise to form a light green precipitate. The solutions were stirred for two hours at room temperature before heating to dryness at 80°C. Materials are abbreviated $M_xPMo_{11}VPyr$, similar to those prepared from $H_3PMo_{12}O_{40}$.

6.1.3 $PMMo_{11}Pyr$ (M = Fe, Ga, Sb, Nb)

Polyatom substitution of phosphomolybdic acid was performed according to known methods for the cations niobium, iron, and antimony.[1,4-6] Substitution with gallium was adapted from the procedures for iron and antimony since both antimony and iron substitutions are performed with ions in oxidation state three. A solution of 5.0 g $H_3PMo_{12}O_{40}$ in 28 mL water was basified to pH = 4.4 with lithium carbonate (Aldrich, 99+%) to form the lacunary Keggin structure $PMo_{11}O_{39}^{7-}$. One molar equivalent of iron(III) nitrate hydrate (Aldrich, 98%), gallium(III) nitrate hydrate (Aldrich, 99.9%), potassium anitmonyl tartrate hemihydrate (Acros, 99%), or niobium oxalate (H.C. Starck, 20.5% wt niobium) was quickly added. The solutions were then allowed to stir at room temperature for two hours before filtering to remove any insoluble product. Pyridine, 0.230 g, was added until a yellow precipitate (blue for antimony substitution) was formed. A large excess of pyridinium chloride, 8 – 9 g, was then added to the solution to increase yield. The solids were separated by centrifugation and washed by three 100 mL aliquots of water.

6.1.4 $M_xP[Fe, Ga, Sb, Nb]Mo_{11}Pyr$ (M = V, Nb, Sb)

Polyatom substitution was performed as described above. However, prior to the addition of pyridine and pyridinium chloride, solutions of vanadyl oxalate (0.023 g/1 g water), niobium oxalate (0.065 g/1 g water), or potassium antimonyl tartrate hemihydrate (0.5 g/1 g water) were added to achieve the desired ratio of exchange metal to Keggin unit. The solutions were stirred at room temperature for one hour to achieve a cloudy green slurry. Pyridine and pyridinium chloride were then added as described above.

6.1.5 $Nb_{0.68}PW_{11}VPyr$

Synthesis of niobium exchanged phosphor—tungstic acid was performed by Alex Blanc in our laboratory following known procedures.[7,8] Sodium metavanadate (Fluka, 98%), 0.764 g, was dissolved in 12.53 g water to obtain a clear solution. The metavanadate solution was added to a clear solution of 0.887 g sodium hydrogen phosphate (Aldrich, anhydrous) dissolved in 12.50 g water and acidified with 0.65 mL sulfuric acid (J.T. Baker, 95% - 99%). A clear reddish-brown solution was obtained and allowed to stir for 20 minutes at room temperature. Following dropwise addition of 22.690 g sodium tungstate dihydrate (Aldrich, 99%) dissolved in 20.99 g water over 50 minutes, the solution was acidified with sulfuric acid to pH 1.47 and refluxed for two hours before cooling to room temperature and extracted with ether. The orange-red lower phase was set aside. The middle phase was acidified with 100 mL of 50 vol% water 50 vol% sulfuric acid before re-extraction with 200 mL ether. The orange-red lower phase was set aside and the middle phase was separated twice more with 100 mL ether, retaining the orange-red bottom phases. The orange-red product phases were combined. Residual ether was removed by an air stream overnight followed by room temperature vacuum treatment for one day. Yield was 16 g of light orange solid. Structure was verified by XRD, ^{31}P NMR in D_2O (major peak at -13.915ppm of $PW_{11}VO_{40}$, very minor peaks at -13.407ppm and -14.292ppm of $PW_{10}V_2O_{40}$ and $PW_{12}O_{40}$, respectively), and FTIR (ν_{as} (P-O) 1069 and 1095 cm^{-1}, ν_{as} (W-O) 966 and ~980 cm^{-1} shoulder, ν_{as} (W-O-W) 887 and 806cm^{-1}). Niobium and pyridine exchange were performed as previously described.

6.1.6 Catalytic studies

Oxidation experiments were performed in a BTRS Jr. single pass vertical reactor system (Autoclave Engineers), Figure 6.1. Reactive flows consisted of a hydrocarbon: ethane (Matheson, 99.9%), ethylene (Matheson, 99.5%), or ethanol (Aaper Alcohol, 100%) mixed with oxygen (Air Liquide, 99.5%), 5% argon in helium (Air Liquide, 99.999%), and steam. Steam was fed as liquid water via syringe pump and vaporized at 150°C by a mixing assembly, Figure 6.2. When ethanol was used as the hydrocarbon feed, it was pumped into the system with water. Empirical flow rates were 4:2:4:5 mL/min hydrocarbon:oxygen:argon/helium:steam. Total pressure was atmospheric. Standard reaction temperature was 380°C. The reactor cabinet and transfer lines were heated to 150°C.

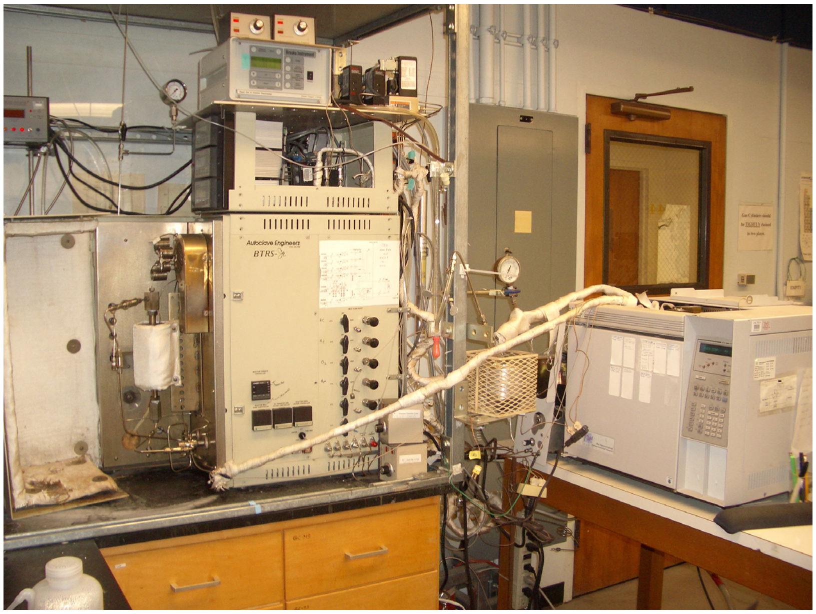

Figure 6.1: Autoclave engineers reactor system with online HP GCD Plus GCMS.

Ethane was oxidized over 0.6 g catalyst sieved to 35-60 mesh and dispersed in 1 mL silicon carbide (16 mesh, Abrasives unlimited) to give a total catalyst bed volume of 1.6 mL. Ethylene and ethanol were oxidized over 0.3 g catalyst diluted to 0.8 mL with silicon carbide. Feeding reactive mixtures over a silicon carbide blank at reaction temperature showed no oxidation activity for butane, propane, ethane, ethane and ethylene, ethylene, or ethanol hydrocarbon feeds. Reproducibility was established over a series of five identical ethane oxidation catalysts. Standard deviation in conversion and space time yield to ethylene or acetic acid was less than 1%. The standard deviation for selectivity data was less than 2%.

Prior to reaction, catalysts were activated in—situ under 300 mL/min helium by ramping from 30°C to 420°C over 5 hours and holding at 420°C for 8 hours (ethylene, ethanol) or 10 hr (ethane) before a 0.67 K/min ramp to reaction temperature. Thermal treatment at 420°C is required for the removal of pyridine and reduction of the catalyst to its active state.[9]

Reactive flows were equilibrated for one hour over the catalyst bed before gas sampling was initiated. A reactor bypass valve was installed allowing the reactive stream an additional hour to equilibrate offline prior to introduction to the catalyst bed (Fig. 6.2). Gas products were analyzed by online GCMS (HP GCD Plus) equipped with a Plot-Q capillary column. Samples were introduced at 120°C for two minutes before ramping at 10 K/min to 265°C and holding for 5 minutes. Oxygenated products were trapped at -78°C and analyzed offline by GCMS or HPLC. Products were separated by HPLC over a Prevail C18 5u 250 mm column using a mobile phase of 1% acetonitrile, 99% 25 mM potassium dihydrogen phosphate solution acidified to pH 2.5 by ortho-phosphoric acid. Products were detected by a UV-VIS diode array detector at 210 nm, 254 nm or 290 nm.

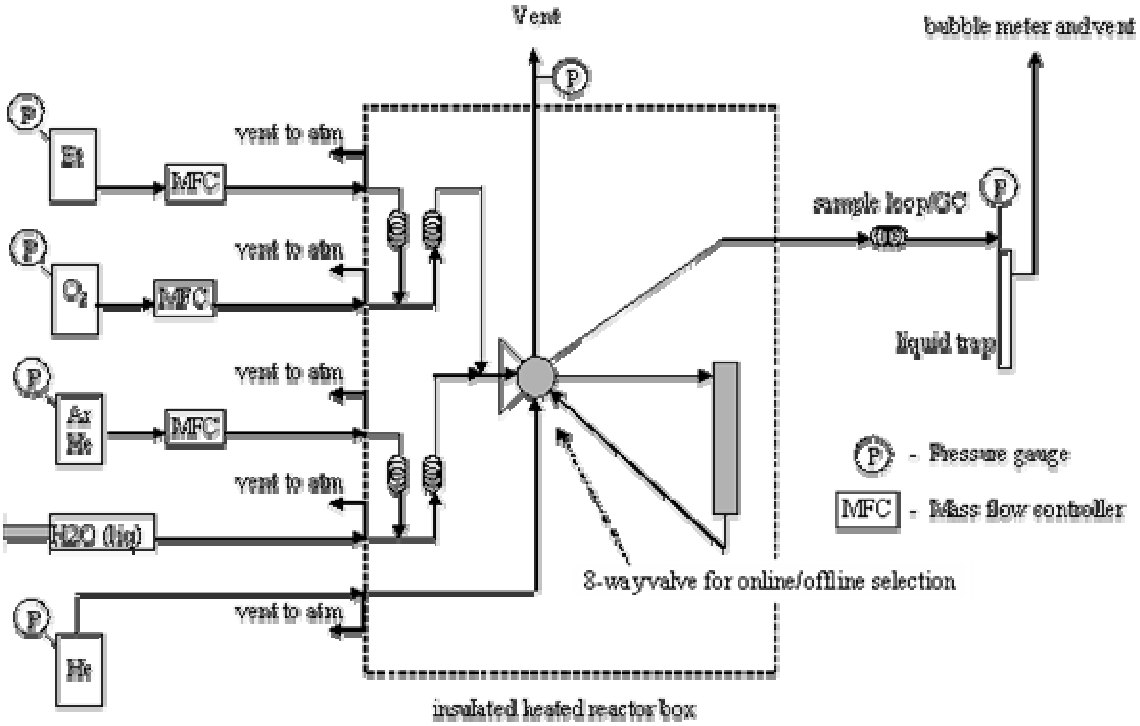

Figure 6.2: Flow diagram for Autoclave Engineers reactor system with bypass valve used for ethane, ethylene, and ethanol reactivity studies.

6.1.7 Characterization

A Netzsch STA 449C Jupiter system was used to record simultaneous thermogravimetric analyses (TGA) and differential scanning calorimetry (DSC). Samples were loaded into platinum/rhodium crucibles and heated to 700^{o}C at 10 K/min under 50 mL/min inert gas. Infrared spectra were taken on a Nicolet Nexus 470 FTIR spectrometer using KBr wafers of approximately 1 wt% solid in KBr.

Powder X-ray diffraction (XRD) was performed on a Scintag XDS 2000 diffractometer using a liquid nitrogen cooled germanium crystal or scintillation detector and CuKα radiation.

Solid—state magic angle spinning (MAS) spectra were obtained on a Bruker Avance 500 spectrometer at a spinning rate of 8, 10, or 12 kHz. ^{31}P NMR spectra were taken at 202.5 MHz against a 85% phosphoric acid standard. ^{69}Ga spectra were acquired at 120.0 MHz against a 1 M gallium(III) nitrate solution. Samples activated offline under helium were transferred to NMR rotor in a nitrogen atmosphere glove box to avoid exposure to moisture and oxygen.

6.2 Characterization Results

6.2.1 Onset of MoO_2 phase transition

TGA analyses of $Nb_xPMo_{11}VPyr$ and $Nb_xPMo_{12}Pyr$ under argon to 700^{o}C were conducted and the position of the exothermic peak due to the phase transition to MoO_2 was plotted as a function of Nb/P in Figure 6.3. Weight loss assignments have been made elsewhere.[9] Doubling the sample size from 20 mg to 40 mg in the TGA resulted in less than a five degree shift in peak position. Since typical sample size was between 15 and 25 mg, differences in peak position greater than four degrees can be considered significant. Introduction of niobium to the catalysts tends to decrease the temperature of phase transition, but not in a linear fashion with niobium loading. For the case of $Nb_xPMo_{12}Pyr$, the temperature of phase transition decreases to 575°C until Nb/P = 0.4, after which the transition is unaffected by niobium loading until Nb/P = 1. At this point there is a sharp decrease to 557°C. For $Nb_xPMo_{11}VPyr$, the temperature of phase transition decreases to 558°C at Nb/P = 0.4, but then increases to 565°C for Nb/P = 0.68 and 0.85. Like $Nb_xPMo_{12}Pyr$, there is a sharp decrease in phase transition temperature to 554°C at Nb/P = 1.0. Although very little MoO_2 is evident in the x-ray diffraction pattern of thermally treated samples (data not shown), the change in onset of MoO_2 phase transition with niobium may indicate differences in phase composition of the active state of the catalyst.

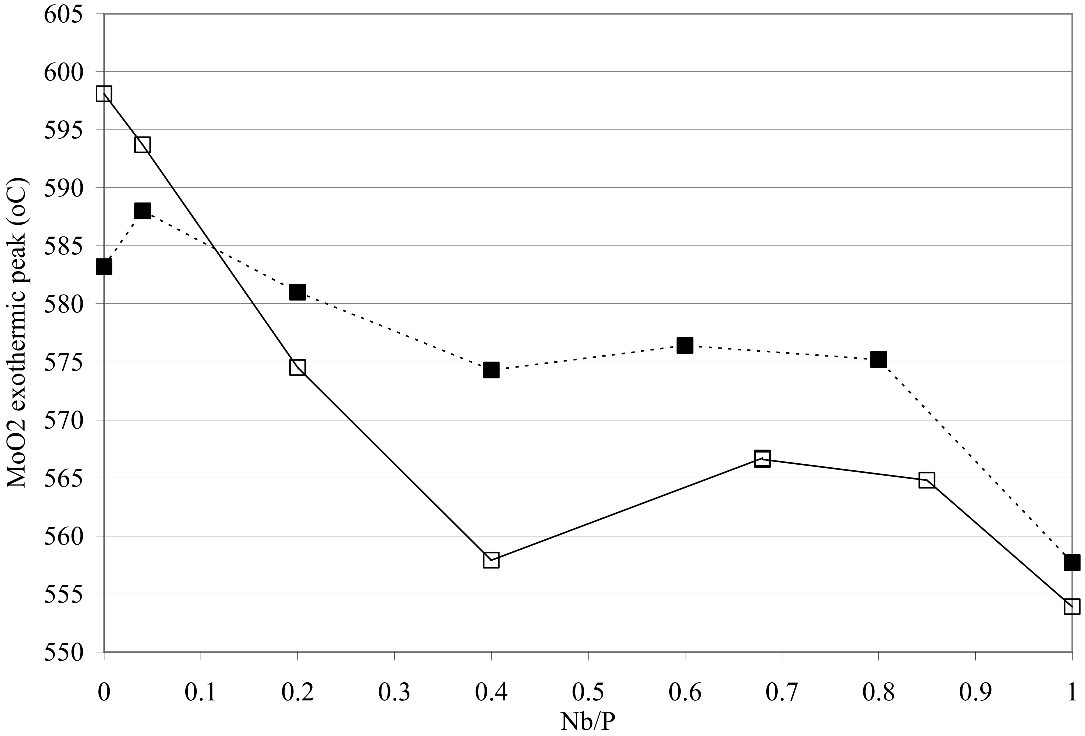

Figure 6.3: Onset of MoO_2 phase transition as measured by TGA-DSC for $Nb_xPMo_{12}Pyr$ (■) and $Nb_xPMo_{11}VPyr$ (□).

6.3 Results of Ethane Oxidation

6.3.1 Effect of Nb source

Catalytic results from $Nb_{0.4}PMo_{11}VPyr$ catalysts synthesized with commercially supplied niobium oxalate and niobium oxalate prepared from niobium pentachloride were compared to verify that differences in niobium source were not the cause of variations in experimental results. Results are found in Table 6.1. The source of niobium has no effect on the catalytic activity.

Nb source	Conversion (%)		Selectivity (%)			STY	
	C_2H_6	O_2	COx	C_2H_4	AcA	C_2H_4	AcA
a	5.1	16.3	55	35	10	0.018	0.005
b	5.0	16.0	54	39	12	0.020	0.005

Table 6.1: Comparison of reactivity data from ethane oxidation over $Nb_{0.4}PMo_{11}VPyr$ prepared from a) commercially supplied niobium oxalate, and b) niobium oxalate prepared from niobium pentachloride. STY = space time yield (mmol/min/g_{cat}).

6.3.2 Effect of Nb/P ratio

The addition of a charge compensating ion to phosphomolybdic acids partially replaces charge balancing protons associated with the Keggin structure. Some of these protons will be used to protonate added pyridine to form pyridinium ions. Adjusting the amount of charge compensating ion, it should be possible to adjust the available protons and affect the number of protons remaining after pyridine exchange. Thus, by adjusting the amount of charge compensating ion, it should be possible to adjust the acidity of the catalyst. It has been shown previously that both niobium and pyridine are essential for active and selective ethane oxidation over Keggin type phosphomolybdic acids.[2] Substitution of vanadium for a framework molybdenum also produces an active and selective oxidation catalyst[1] and has been shown to increase selectivity to acetic acid and ethylene at the expense of overall ethane conversion.[2] Studies of butane oxidation suggest that activity and selectivity are sensitive to Nb/P ratio.[1] Preliminary ethane studies suggest that ethane oxidation might also be sensitive to Nb/P ratio.[2] Those types of studies have been repeated for ethane oxidation over both niobium exchanged phosphomolybdic and vanado—phosphomolybdic acids. The results are given in Figure 6.4 and Tables 6.2 and 6.3.

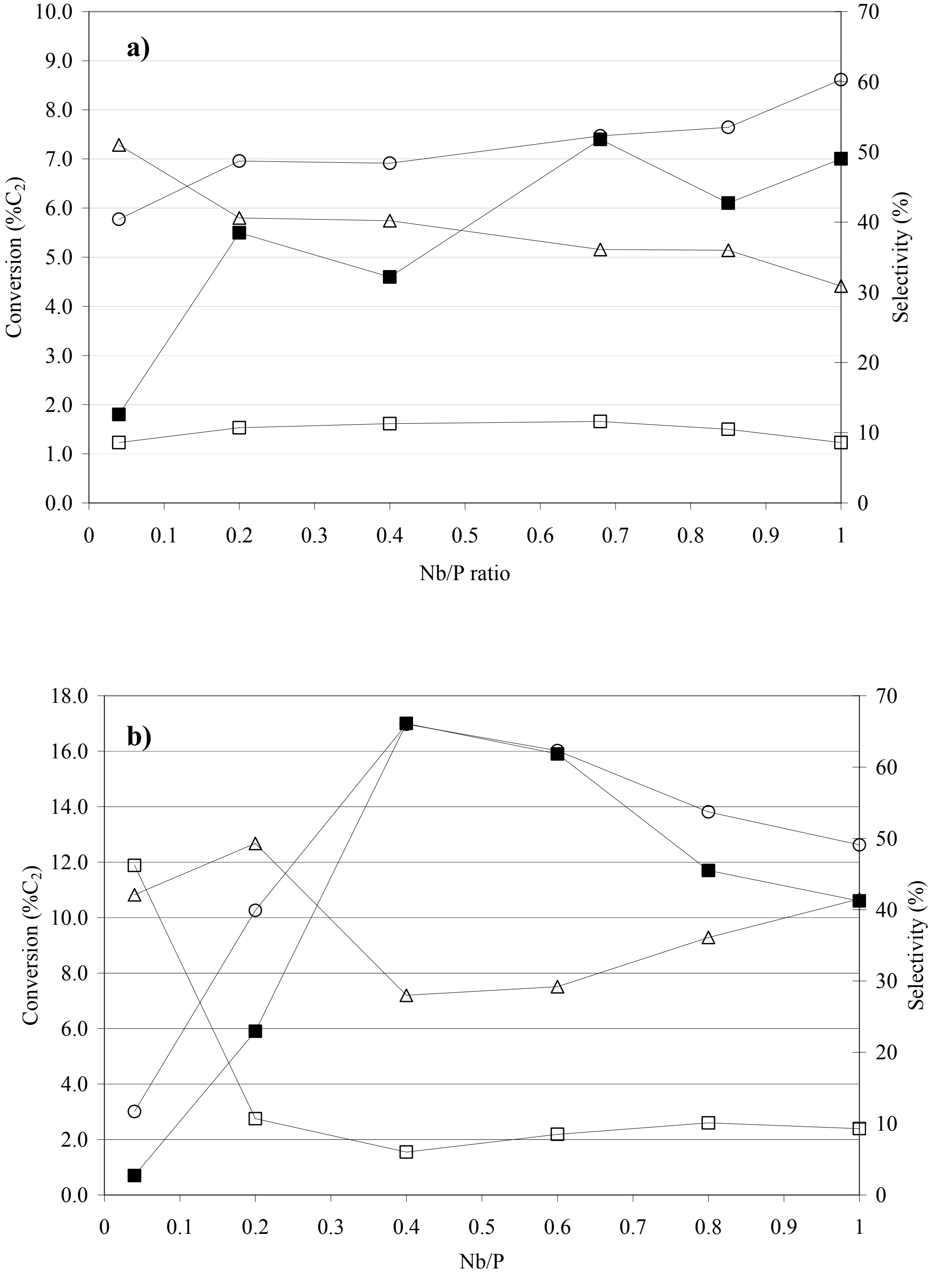

Figure 6.4: Ethane oxidation as a function of Nb/P ratio for a) $Nb_xPMo_{11}VPyr$ and b) $Nb_xPMo_{12}Pyr$; ■ = conversion, ○ = selectivity to CO_x, Δ = selectivity to ethylene, □ = selectivity to acetic acid.

Nb/P	Conversion (%)		Selectivity (%)			STY	
	C_2H_6	O_2	CO_x	C_2H_4	AcA	C_2H_4	AcA
0.04	1.8	6	40	51	9	0.010	0.002
0.2	5.5	18	49	41	11	0.023	0.006
0.4	4.6	14	48	40	11	0.018	0.005
0.68	7.4	24	52	36	12	0.022	0.007
0.85	6.1	22	54	36	11	0.022	0.007
1	7.0	26	60	31	9	0.020	0.006

Table 6.2: Reactivity data for ethane oxidation over $Nb_xPMo_{11}VPyr$. STY = space time yield (mmol/min/g_{cat}).

Nb/P	Conversion (%)		Selectivity (%)			STY	
	C_2H_6	O_2	CO_x	C_2H_4	AcA	C_2H_4	AcA
0.04	0.7	2	12	42	46	0.003	0.004
0.2	5.9	17	40	49	11	0.030	0.006
0.4	17.0	71	66	28	6	0.049	0.010
0.6	15.9	58	62	29	9	0.053	0.015
0.8	11.7	40	54	36	10	0.050	0.014
1	10.6	34	49	42	9	0.048	0.011
0.4*	4.7	12.1	30.2	61.7	8	0.033	0.004

* exchanged with pyridinium chloride instead of pyridine

Table 6.3: Reactivity data for ethane oxidation over $Nb_xPMo_{12}Pyr$. STY = space time yield (mmol/min/g_{cat}).

Consistent with previous studies, data in Figure 6.4 demonstrate that polyatom substitution of molybdenum for vanadium results in decreased activity towards ethane at all niobium loadings. Selectivity to ethylene is slightly enhanced for $Nb_xPMo_{11}VPyr$ over $Nb_xPMo_{12}Pyr$ catalysts at niobium loadings between 0.2 and 0.8 Nb/P. Selectivity to acetic acid is nearly identical in both cases for Nb/P > 0.2. The results given in Figure 6.4a and Table 6.2 for the vanadium containing catalysts indicate that there is no clear maximum for the production of ethylene and acetic acid. Space time yields between 0.018mmol/min/g_{cat}

ethylene and 0.005 to 0.007 mmol/min/g_{cat} acetic acid were observed for Nb/P between 0.2 and 1.0. This is contrary to previous findings, which showed a maximum in space time yield to acetic and ethylene at Nb/P = 0.87.[2] Data listed in Figure 6.4b and Table 6.3 indicate that without vanadium substitution, conversion reaches a maximum of 17.0% at Nb/P = 0.4, but space time yield is maximized at Nb/P = 0.6 (0.053 and 0.015 mmol/min/g_{cat} ethylene and acetic acid, respectively). Selectivity to over-oxidation products CO_x is also maximized at Nb/P = 0.4. This is consistent with previous studies.

Figure 6.5 presents an overlay of selectivity versus conversion for the data collected in the niobium loading series experiments. It is worthwhile to note that except for very low conversion in the case of the $Nb_xPMo_{12}Pyr$ series, the selectivity to ethylene decreases roughly linearly with increasing conversion. Conversely, the selectivity to deep oxidation productions CO_x increases linearly with increasing conversion for either catalyst series. The selectivity to acetic acid is roughly constant with conversion. Thus, in both the $Nb_xPMo_{11}VPyr$ and the $Nb_xPMo_{12}Pyr$ samples the effect of niobium is to shift the reaction products along the selectivity curve, although not monotonically with Nb/P ratio. It is also clearly evident from the data in Figure 6.5 that the vanadium substituted catalysts exhibit higher selectivity to over oxidation products CO_x and lower selectivity to ethylene at the same level of conversion as catalysts without vanadium. The only exception is at very low conversions. From these data and those given in Tables 6.2 and 6.3, it can be concluded that substitution of vanadium for molybdenum in the Keggin ion both inhibits catalytic activity and shifts the selectivity towards over-oxidation products.

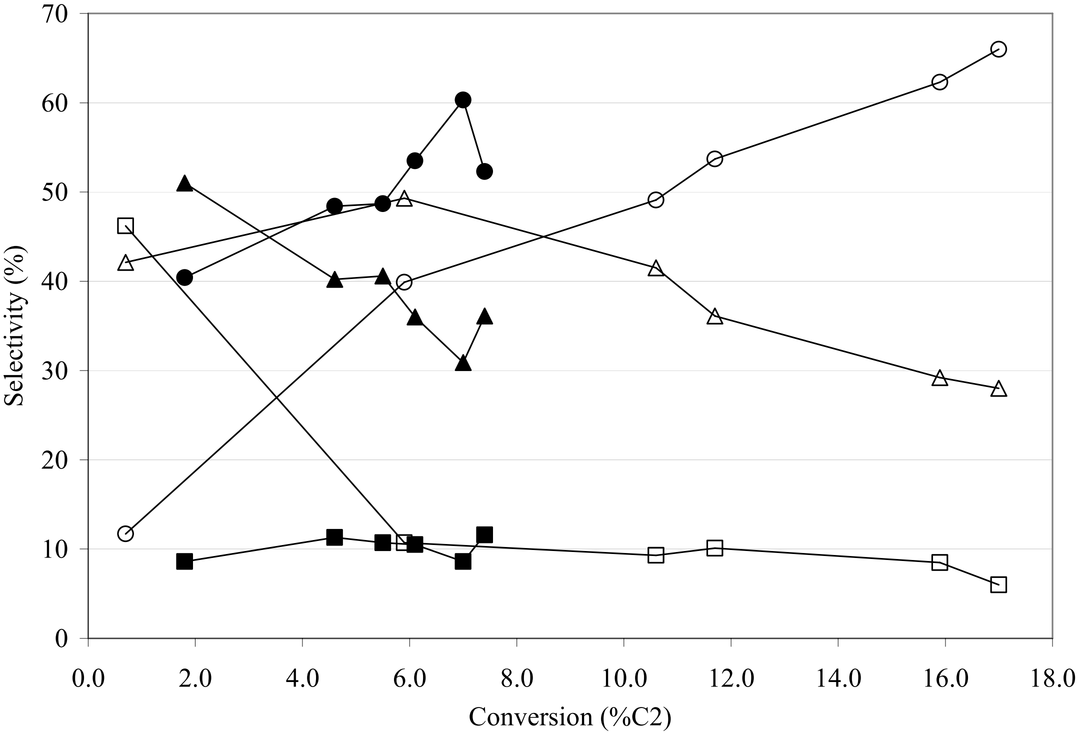

Figure 6.5: Selectivity versus conversion for $Nb_xPMo_{11}VPyr$ (filled markers) and $Nb_xPMo_{12}Pyr$ (hollow markers); ●,○ = selectivity to CO_x, ▲ ,Δ = selectivity to ethylene, ■,□ = selectivity to acetic acid.

Attempts at correlating ^{31}P SS MAS NMR decomposition peaks after thermal treatment without exposure to oxygen and moisture to Nb/P ratio and catalytic activity were unsuccessful.

6.3.3 Effect of pyridinium

The importance of pyridine protonation during catalyst synthesis was probed by using pyridinium chloride instead of pyridine during catalyst synthesis. In this manner, the amount of protons in the heteropolyanion following niobium exchange would not be altered by addition of the organic. Results in Table 6.3 show that when pyridinium chloride is used instead of pyridine during catalyst synthesis, the activity of the catalyst is greatly reduced. However, the use of pyridinium chloride does not fundamentally change the function of the catalyst. Examining the selectivities and space time yields, it becomes evident that the use of pyridinium chloride simply shifts the reactivity profile of the catalyst along the selectivity versus conversion curve (Fig. 6.5) constructed from the results of varying Nb/P ratio.

6.3.4 Effect of Temperature

Results of ethane oxidation studies over $Nb_{0.4}PMo_{12}Pyr$ conducted at 380, 360 and 340°C are presented in Table 6.4. As temperature is decreased, conversion of ethane decreases from 18% at 380°C to just 7% at 340°C. Concomitantly, selectivity to CO_x drops from 66 to 41% while selectivity to ethylene and acetic acid increases from 28 and 6% to 46 and 13%, respectively. Despite the increase in selectivity for both ethylene and acetic acid, decreased conversion results in a 35% reduction of space time yield for ethylene and a 18% reduction for acetic acid. The temperature dependence of space time yield indicates that ethylene production is a stronger function of temperature than acetic acid production. However, the high selectivity to carbon oxides at 340°C may mask the intrinsic rate of production of either product. Thus, it can only be suggested that this result is consistent with the belief that oxidative dehydrogenation of ethane to ethylene and acetic acid occurs through an initial ethoxy intermediate which yields ethylene through β-H elimination (high temperature) and acetic acid through α-H eliminations (low temperature).[10,11]

T (^oC)	Conversion (%)		Selectivity (%)			STY	
	C_2H_6	O_2	COx	C_2H_4	AcA	C_2H_4	AcA
380	18	73	66	28	6	0.049	0.011
360	12	43	54	37	9	0.041	0.010
340	7	22	41	46	13	0.032	0.009

Table 6.4: The effect of temperature on ethane oxidation over $Nb_{0.4}PMo_{12}Pyr$. STY = space time yield ($mmol/min/g_{cat}$).

6.3.5 Effects of steam

Numerous reports highlight the beneficial effect of steam on the oxidation of ethane to acetic acid.[11-15] These studies suggest the possibility of an optimal steam partial pressure for the oxidation of ethane. Studies varying steam flow from 8% to 50% of the feed were conducted while maintaining a constant space velocity. Results for $Nb_{0.6}PMo_{12}Pyr$ at space velocities of 2250 and 4500 h^{-1} are presented in Table 6.5. Conversion at either space velocity is roughly constant until 33% steam feed. Selectivity to carbon oxides decreases as steam is increased, while selectivities to ethylene and acetic acid are enhanced. The production of both acetic acid and ethylene passes through a maximum at 33% steam due to decreasing conversion. These trends are repeatable at either 2250 or 4500 h^{-1} gas hourly space velocity. Although water is required for the formation of acetic acid, it is also a product of ethylene formation and, at high steam feed, may compete for adsorption sites on the catalyst surface.[13] Excess steam may therefore limit ethane conversion to ethylene and prevent further adsorption of ethane. Thus, production of ethylene and acetic acid are maximized at 33% steam under hydrocarbon rich conditions.

GHSV (h^{-1})	Steam (mL)	Conversion (%)		Selectivity (%)			STY	
		C_2H_6	O_2	COx	C_2H_4	AcA	C_2H_4	AcA
2250	5	14	53	69	27	4.8	0.039	7.0E-03
	10	12	45	66	27	7.1	0.034	9.1E-03
	20	15	55	60	31	8.3	0.051	1.4E-02
	30	9	30	52	36	12.0	0.033	1.1E-02
4500	5	7	24	62	35	3.7	0.048	5.1E-03
	10	6	21	57	38	5.7	0.046	7.0E-03
	20	7	24	54	40	6.2	0.058	8.9E-03
	30	5	18	47	45	8.0	0.048	8.5E-03

Table 6.5: Effect of steam flow on ethane oxidation over $Nb_{0.6}PMo_{12}Pyr$ at constant total flow of 60 mL/min. STY = space time yield (mmol/min/g_{cat}).

6.3.6 Effects of ethane:oxygen ratio

Preliminary studies have indicated that the catalysts under investigation perform best in hydrocarbon rich environments.[1,16] A secondary study showed that the catalysts are also sensitive to the ethane/oxygen ratio in the hydrocarbon rich regime.[2] It is difficult to interpret these results due to variations in space velocity. Table 6.6 presents data from ethane oxidation over $Nb_{0.6}PMo_{12}Pyr$ at 380°C and constant space velocity while varying the ethane to oxygen ratio from 0.5 (oxidizing environment) to 5 (reducing environment). The amount of carbon oxides decreases from 68 to 60% as the reactive environment becomes more reducing. Concomitantly, selectivity to ethylene increases from 23 to 30% while selectivity to acetic acid remains roughly constant. Conversion reaches a maximum value of 17% at ethane to oxygen ratio of two. No deactivation of catalyst was observed over the time frame of the experiment (6 hours). Thus, the catalyst surface is able to support a fairly reducing environment while maintaining production of both ethylene and acetic acid.

Flow (He:O_2:C_2:steam)	**C_2:O_2**	**Conversion (%)**		**Selectivity (%)**			**STY**	
		C_2H_6	**O_2**	**COx**	**C_2H_4**	**AcA**	**C_2H_4**	**AcA**
16:16:8:20	0.5	13	13	68	23	9	0.014	5.4E-03
16:8:16:20	2	17	61	64	25	10	0.042	1.7E-02
16:4:20:20	5	13	97	60	30	10	0.048	1.5E-02

Table 6.6: Effect of ethane/oxygen ratio at constant space velocity for ethane oxidation over $Nb_{0.6}PMo_{12}$Pyr. STY = space time yield (mmol/min/g_{cat}).

6.3.7 Polyatom substitution

The redox properties of heteropolyanions depend on the identity and location of substituted transition metals.[17-20] The effect of charge-compensating cation and heteroatom substitution in pyridine exchanged phosphomolybdic acids has been investigated for the oxidation of light alkanes for a series of transition metals.[1,2] These studies found that in all cases, a phosphorous heteroatom and the presence of niobium yielded the best performing catalysts. Selective propane oxidation was further enhanced by the presence of a vanadium polyatom.[1] Studies of polyatom substitution beyond vanadium have not been performed for ethane oxidation.

It has been reported that the addition of iron(III) cations to cesium hydrogen salts of molybdophosphoric acids enhances catalytic activity towards ethylene from ethane,[4,21] while polyatom substitution of iron for molybdenum results in enhanced catalytic activity for the oxidative dehydrogenation of 2-propanol.[4,22] Gallium oxides are well known for their ability to promote partial oxidation of propane to propylene in a variety of systems.[23-25] Addition of gallium(III) cations to cesium salts of vanado-phosphomolybdic acids results in improved oxidation of propane to acrylic acid, propylene, and acetic acid.[26] Polyatom substitution of antimony for molybdenum in potassium/ammonium salts of molybdophosphoric acids stabilizes catalytic activity with time for ethane oxidation and leads to increased thermal stability of the heteropolyanion.[5] Thus, antimony, iron, and gallium were chosen to extend the studies of polyatom substitution in phosphomolybdic acids for the selective oxidation of ethane.

Table 6.7 presents ethane oxidation data for a series of Keggin heteropolyanions including iron, gallium, or antimony polyatoms with and without charge compensating cations of vanadium or niobium. Acid forms $PMo_{11}XPyr$ (X = iron, gallium) show less than one percent conversion of ethane. In the case of iron polyatom substitution, selectivity is completely to acetic acid. Addition of vanadium as a charge compensating ion very slightly increases catalytic activity. In the case of iron polyatom substitution selectivity of acetic acid is reduced to 33%, while carbon oxides and ethylene are produced with 43 and 24% selectivity, respectively. If niobium is used as a charge-compensating cation in place of vanadium, a drastic increase in catalytic activity is observed. Conversion for both $Nb_{0.5}PMo_{11}XPyr$ (X = iron or gallium) increases to 18% ethane. Product distributions for the iron and gallium substituted catalysts are nearly identical to $Nb_{0.4}PMo_{12}Pyr$ with carbon oxides as the major product (69, 65% selectivity, respectively) followed by ethylene (25, 30% selectivity, respectively), and finally acetic acid (6, 5% selectivity, respectively). However, taken in conjunction with space time yield, gallium polyatom substitution improves the production of ethylene at the expense of carbon oxides over both $Nb_{0.4}PMo_{12}Pyr$ and $Nb_{0.5}PMo_{11}FePyr$.

Catalyst	**Conversion (%)**		**Selectivity (%)**			**STY**	
	C_2H_6	**O_2**	**COx**	**C_2H_4**	**AcA**	**C_2H_4**	**AcA**
$PMo_{11}FePyr$	0.5	1.6	0	0	100	-	4.7E-03
$PMo_{11}GaPyr$	0	0	0	0	0	-	-
$(VO)_{0.5}PMo_{11}FePyr$	0.9	3.3	43	24	33	0.002	3.2E-03
$(VO)_{0.5}PMo_{11}GaPyr$	0.4	1.5	0	0	100	-	4.6E-03
$Nb_{0.5}PMo_{11}FePyr$	18	67	69	25	6	0.044	9.9E-03
$Nb_{0.5}PMo_{11}GaPyr$	18	67	65	30	5	0.059	8.6E-03
$Nb_{0.5}PMo_{11}SbPyr$	9	29	53	40	8	0.034	6.4E-03
$Nb_{0.40}PMo_{12}Pyr$	17	71	66	28	6	0.049	9.9E-03
$Nb_{0.68}PMo_{11}VPyr$	7	24	52	36	12	0.022	7.1E-03
$(VO)_{0.5}PMo_{11}NbPyr$	11	42	61	31	8	0.040	1.0E-02

Table 6.7: The effect of polyatom substitution and cation exchange on ethane oxidation. STY = space time yield (mmol/min/g_{cat}).

Polyatom substitution with antimony, combined with a niobium charge-compensating cation, reduces catalytic activity by a factor of two when compared to the equivalent iron and gallium polyatom substituted samples. However, the catalytic activity is similar to vanadium substituted catalysts. Conversion falls to 9% with selectivities of 53, 40 and 8% to carbon oxides, ethylene, and acetic acid, respectively. These values do not fit on either selectivity/conversion curve presented for $Nb_xPMo_{11}VPyr$ and $Nb_xPMo_{12}Pyr$ in Figure 6.5.

Examination of all the data presented in Table 6.7 indicates that meaningful catalytic activity can only be obtained when niobium is present in the catalyst in either a charge-compensation capacity or as a polyatom. The most active catalysts tend to have niobium as an exchange cation rather than a polyatom.

To further explore the importance of antimony polyatom substitution relative to the presence of niobium, the Nb/P ratio was varied for antimony polyatom substituted catalysts. A mirror image of the experiment, swapping the positions of antimony and niobium, was also conducted as a control. Data are presented in Table 6.8. Except at the lowest X/P (X = Sb, Nb) ratio, the selectivity profiles of either catalyst are very similar with carbon oxides and ethylene accounting for ~50 and ~45% at all values of X/P, respectively. Selectivity to acetic acid was slightly enhanced at low X/P for antimony polyatom catalysts. At X/P = 0.15, the presence of antimony in the polyatom position decreases over—oxidation to carbon oxides. A maximum conversion of 9% at 380°C was observed over $Nb_{0.5}PMo_{11}SbPyr$ versus 7% conversion over $Sb_{0.5}PMo_{11}NbPyr$. Thus, when niobium is present, the catalytic selectivity profile is a very weak function of X/P ratio. These data indicate that niobium is dominating the reactivity of the catalysts, as opposed to the X/P ratio or the Nb/Sb ratio.

Catalyst	**Conversion (%)**		**Selectivity (%)**			**STY**	
	C_2H_6	**O_2**	**COx**	**C_2H_4**	**AcA**	**C_2H_4**	**AcA**
$Nb_{0.15}PMo_{11}SbPyr$	5	16	47	45	8	0.024	4.3E-03
$Nb_{0.5}PMo_{11}SbPyr$	9	29	53	40	8	0.034	6.4E-03
$Nb_{1.0}PMo_{11}SbPyr$	2	6	49	49	2	0.011	4.0E-04
$Sb_{0.15}PMo_{11}NbPyr$	7	26	63	32	5	0.024	4.0E-03
$Sb_{0.5}PMo_{11}NbPyr$	7	24	53	43	5	0.031	3.5E-03
$Sb_{1.0}PMo_{11}NbPyr$	3	9	54	43	3	0.012	1.1E-03
$Nb_{0.5}PMo_{11}SbPyr$*	11	35	50	45	5	0.050	5.9E-03
$Sb_{0.5}PMo_{11}NbPyr$*	6	16	40	56	4	0.032	2.2E-03

Table 6.8: The effect of Nb/P and Sb/P on ethane oxidation; * indicates data collected at 400°C reaction temperature.

Plotting space time yield as a function of X/P demonstrates the competition between conversion and selectivity for the above series of catalyst and further illustrates that the presence of niobium is dominating the reactive behavior of the catalyst. The plot is presented in Figure 6.6. Since the activity of niobium and antimony polyatom substituted catalysts are most similar to vanadium polyatom substituted catalysts, the activity of $Nb_{0.68}PMo_{11}VPyr$ is plotted as a comparison. It is apparent that production of ethylene and acetic acid is a function of X/P, but not of the identity of X for X = antimony, niobium. At X/P of 0.68, it appears that vanadium would be less active for the production of ethylene, but would be more active for the production of acetic acid.

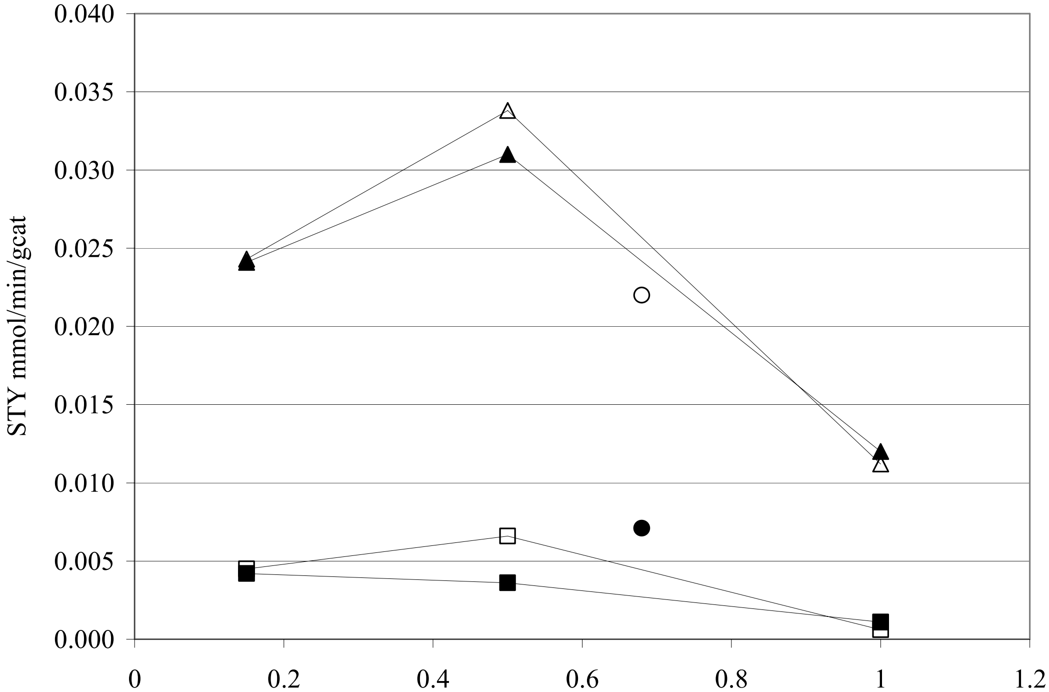

Figure 6.6: Space time yield of ethylene (▲, X = Sb; Δ, X = Nb; ○, X = vanadium) and acetic acid (■, X = Sb; □, X = Nb; ●, X = vanadium).

Some benefit of antimony polyatom substitution is evident when the reaction temperature is raised from 380 to 400^{o}C. Data are included in Table 6.8. Ethane conversion increases to 11% for $Nb_{0.5}PMo_{11}SbPyr$ but decreases to 6% for $Sb_{0.5}PMo_{11}NbPyr$. The selectivity profile of $Nb_{0.5}PMo_{11}SbPyr$ is unaffected resulting in increased ethylene production (0.050 versus 0.034 mmol/min/g_{cat} at 400 and 380^{o}C, respectively). Thus, it appears the antimony stabilizes the reaction at elevated temperatures when it is present as a polyatom.

Iron is thought to improve catalytic activity of cesium salts of heteropolyanions in reducing or oxidizing environments by aiding in the re-oxidation or reduction of the catalysts, respectively.[4,17,27] Studies of ethane oxidation under oxidizing and reducing environments were completed for $Nb_{0.5}PMo_{11}FePyr$ to determine if the properties of iron extend to the system under investigation. Results are shown in Table 6.9. Comparing the data in Table 6.9 to the data in Table 6.6 it is clear that addition of iron has very little effect in reducing environments other than to reduce the space time yield of acetic acid. Conversion is slightly increased from 13 to 16% using $Nb_{0.6}PMo_{12}Pyr$ under oxidizing conditions while selectivity to carbon oxides remains constant. A slight improvement in ethylene production from 0.014 to 0.017 mmol/min/g_{cat} is evident while space time yield to acetic acid drops from 5.4e-3 to 4.4e-3 mmol/min/g_{cat}. Thus, in the current system, iron does not meaningfully enhance the activity of the catalyst.

Flow (He:O_2:C_2:steam)	C_2:O_2	Conversion (%)		Selectivity (%)			STY	
		C_2H_6	O_2	COx	C_2H_4	AcA	C_2H_4	AcA
16:16:8:20	0.5	16	15	69	25	6	0.017	4.4E-03
16:8:16:20	2	18	67	69	25	6	0.044	1.0E-02
16:4:20:20	5	13	100	63	31	6	0.047	9.9E-03

Table 6.9: Ethane oxidation over $Nb_{0.5}PMo_{11}FePyr$ for various ethane:oxygen ratios. STY = space time yield (mmol/min/g_{cat}).

Variations of steam flow were conducted over $Nb_{0.5}PMo_{11}GaPyr$. Contrary to the behavior of $Nb_{0.6}PMo_{12}Pyr$ (Table 6.5), $Nb_{0.5}PMo_{11}GaPyr$ exhibits a maximum space time yield to ethylene while space time yield to acetic acid passes through a minimum at 33% steam feed (Table 6.10). Ethylene production is enhanced at all steam levels as compared to $Nb_{0.6}PMo_{12}Pyr$, partially due to increased conversion of both ethane and oxygen. Unlike $Nb_{0.6}PMo_{12}Pyr$, oxygen conversion remains constant at around 70% at all steam levels. Selectivity follows the same trend as for $Nb_{0.6}PMo_{12}Pyr$, but carbon oxide production is increased by 5 to 7% at all steam levels. Thus, it appears that gallium may stabilize the catalyst towards water during reaction, with the result of increasing unselective oxidation to carbon oxides.

Steam (mL)	Conversion (%)		Selectivity (%)			STY	
	C_2H_6	O_2	COx	C_2H_4	AcA	C_2H_4	AcA
10	20	73	73	22	5	0.042	9.7E-03
20	18	67	65	30	5	0.059	8.6E-03
30	14	72	60	31	10	0.042	1.3E-02

Table 6.10: Effect of steam flow on ethane oxidation over $Nb_{0.}5PMo_{11}GaPyr$ at GHSV = 2250 h^{-1}. STY = space time yield (mmol/min/g_{cat}).

6.4 Results of ethylene oxidation

6.4.1 Effect of catalyst composition

Ethylene is one possible intermediate of selective ethane oxidation.[10,28] The effect of catalyst composition for ethylene oxidation was studied in an effort to better understand the role of framework and charge-compensating transition metals. As previously discussed, the identity and location of transition metals in the heteropolyanion can be used to tune the redox properties of the catalyst. Furthermore, specific metals are thought to play specific roles in ethylene oxidation. Niobium in the form of niobic acid is extremely efficient for the hydration of ethylene to ethanol.[29] Molybdenum and vanadium are implicated in taking ethylene to acetic acid [11,30] and propylene to acrylic acid in Mo-V-Nb-O_x catalyst systems.[31]

The results of varying Keggin ion composition with niobium, molybdenum, vanadium, and tungsten at GHSV 2250h^{-1} to probe both redox and identity properties are shown in Table 6.11. Consistent with results for propane, butane, and ethane,[1,2] the presence of both niobium and a charge compensating ion other than a proton is required for significant catalytic activity. When both of these conditions are met, both carbon and oxygen conversion are maximized (lines 6-8 in Table 6.11). The pure acid forms are able to produce small amounts of acetic acid (~0.010 mmol/min/g_{cat}). The introduction of a vanadium or niobium polyatom increases conversion without increasing the production of acetic acid. Instead, in the acid form, polyatom substitution of molybdenum with vanadium or niobium results in increased selectivity to carbon oxides from 53% to 78 and

72%, respectively. Niobium polyatom substitution shifts the carbon oxide profile towards completely oxidized CO_2 in both the acid forms (lines 2 and 3) and the cation exchanged forms (lines 7 and 8). Comparison of catalysts containing charge-compensating ions, it is apparent that molybdenum is required, but insufficient on its own to affect significant reactivity (compare lines 4 and 9 to lines 6-8). Furthermore, when niobium is present as a polyatom or charge-compensating cation, the presence of vanadium does not affect reactivity. In all catalysts including both niobium and a charge compensating cation, selectivity to carbon oxides at $380^{o}C$ is very high at ~75%. However, the catalysts produce a large amount of acetic acid, 0.06mmol/min/g_{cat}, which increases to 0.09 and 0.12 mmol/min/g_{cat} as the temperature is lowered to 340 and $300^{o}C$, respectively. The increase in acetic acid is due to a decrease in the amount of carbon oxides, from 75% at $380^{o}C$ to only 53% at $300^{o}C$. Oxygen conversion remains nearly 100% even at $300^{o}C$ while carbon conversion does not decrease. This indicates that further temperature reduction should reduce carbon oxides while maintaining high activity towards acetic acid. Interestingly, small amounts of acrylic and maleic acids were formed. No ethanol was observed.

Catalyst	T (^oC)	Conversion (%)		Selectivity (%)			STY
		C_2H_4	O_2	CO	CO_2	AcA	AcA
$PMo_{12}Pyr$	380	2	6	52	8	41	0.010
$PMo_{11}VPyr$	380	5	18	78	6	16	0.007
$PMo_{11}NbPyr$	380	5	19	58	13	29	0.014
$Mo_{0.68}PMo_{12}Pyr$	380	2	9	65	13	22	0.004
$(VO)_{0.68}PMo_{12}Pyr$	380	3	13	77	5	18	0.005
$Nb_{0.4}PMo_{12}Pyr$	380	31	100	61	14	21	0.059
	340	32	100	51	15	28	0.086
$Nb_{0.68}PMo_{11}VPyr$	380	31	100	63	15	21	0.059
	340	32	97	53	13	30	0.089
$(VO)_{0.50}PMo_{11}NbPyr$	380	27	100	58	18	21	0.058
	340	27	100	45	20	31	0.084
	300	27	96	34	19	44	0.123
$Nb_{0.68}PW_{11}VPyr$	380	4	22	69	27	3	0.001

Table 6.11: Effect of composition on ethylene oxidation at GHSV 2250 h^{-1}. STY = space time yield (mmol/min/g_{cat}).

Examination of catalyst reduction potential lends further insight into the role of the catalyst metals. Following the work of Song et al.,[20] the reduction potentials of $(VO)_{0.68}PMo_{12}Pyr$, $Mo_{0.68}PMo_{12}Pyr$ and the niobium containing cation exchanged catalysts should be approximately equal. However, only the niobium containing catalysts are active. Furthermore, the reduction potentials of $Nb_{0.68}PW_{11}VPyr$ and $Nb_{0.4}PMo_{12}Pyr$ should also be approximately equal, but only the molybdophosphate catalyst is active. Additionally, the inactive polyatom substituted acid forms of the catalysts should have reduction potentials similar to the active niobium containing cation exchanged forms. Consequently, it is apparent that the reduction potential of the catalyst is not the governing factor for ethylene conversion. Instead, catalytic activity is dominated by the identity of the metals present. Specifically, niobium and molybdenum must be present together for significant activity. This suggests a synergy between the two metals in the active state of the catalyst.

6.4.2 Effect of Nb/P ratio

Since the amount of charge compensating ion present can be used to adjust the acidity of the catalyst, studies were conducted to determine if an optimal Nb/P ratio exists for ethylene conversion. In order to obtain meaningful data, space time yield was doubled to 4500 h^{-1} and temperature was dropped to 340 and 300°C. The resulting data are presented in Table 6.12. Even at 340°C and GHSV of 4500 h^{-1}, oxygen conversion is nearly 100% by Nb/P = 0.2, partially confounding interpretation of the data. Space time yield to acetic acid increases until Nb/P = 0.6 where it reaches a maximum of 0.18 mmol/min/g_{cat}. Acrylic acid production is minimized at 0.009 mmol/min/g_{cat} and Nb/P = 0.6 and maximized at 0.017 mmol/min/g_{cat} and Nb/P = 1.0. Maleic acid is also produced at low levels. Decreasing the temperature to 300°C reduces oxygen conversion, allowing the effect of Nb/P ratio greater than 0.2 to be examined. Figure 6.7 presents conversion and selectivity data as a function of Nb/P, illustrating a clear maximum in selectivity to acetic acid of 42% at Nb/P = 0.6 while carbon oxides are minimized at 52% selectivity. Conversion continues to rise with Nb/P ratio, leading to a maximum space time yield of acetic acid of 0.16 mmol/min/g_{cat} at Nb/P = 0.8. Acrylic acid production tends to decrease with Nb/P ratio, but is as high as 0.012 mmol/min/g_{cat} (18% selectivity) at Nb/P = 0.04. Maleic acid is produced at a relatively constant low level of 0.002 mmol/min/g_{cat} regardless of Nb/P ratio. Unlike Nb/P studies of ethane oxidation, selectivities to carbon oxides and acetic acid do not track linearly with conversion. This indicates that niobium may be directly involved in the conversion of ethylene to acetic acid rather than simply a control of acid sites.

Nb/P	**T (°C)**	**Conversion (%)**		**Selectivity (%)**					**STY**		
		C_2H_4	**O_2**	**CO**	**Cox**	**AcA**	**Acr A**	**MA**	**AcA**	**Acr A**	**MA**
0.04	340	11	47	37	56	32	9.1	2.8	0.077	0.014	0.003
	300	4	20	39	61	19	18.4	1.4	0.018	0.012	0.001
0.2	340	24	99	54	73	22	3.9	1.5	0.114	0.014	0.004
	300	16	66	46	64	29	3.8	0.9	0.103	0.009	0.002
0.4	340	27	98	52	64	32	2.5	1.4	0.167	0.009	0.004
	300	13	53	45	56	40	2.6	1.0	0.124	0.005	0.002
0.6	340	26	98	51	68	29	2.2	1.1	0.175	0.009	0.003
	300	14	58	37	52	42	4.9	1.3	0.140	0.006	0.002
0.8	340	26	100	48	65	29	4.0	1.2	0.179	0.016	0.004
	300	18	75	38	56	39	4.4	1.1	0.163	0.012	0.002
1	340	25	96	46	63	31	4.3	1.6	0.182	0.017	0.005
	300	19	46	45	64	32	2.5	1.0	0.141	0.007	0.002

Table 6.12: Effect of Nb/P ratio on ethylene oxidation at GHSV 4500 h^{-1}. Acr A = acrylic acid, MA = maleic acid, STY = space time yield (mmol/min/g_{cat}).

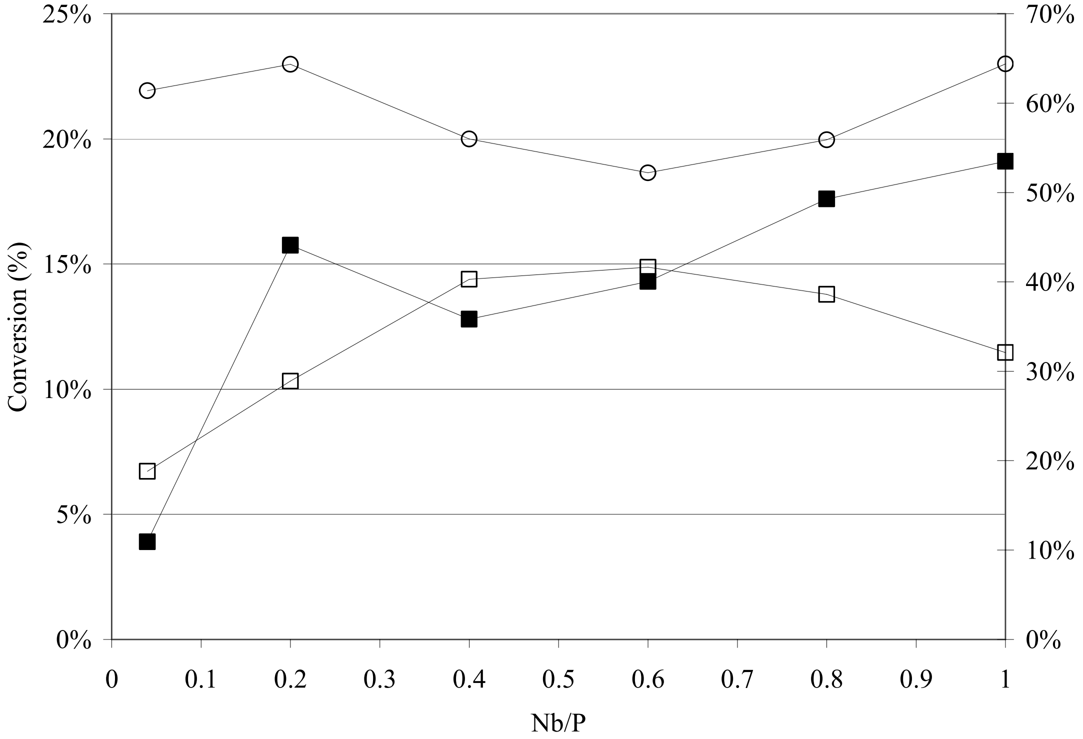

Figure 6.7: Ethylene oxidation as a function of Nb/P ratio for $Nb_xPMo_{12}Pyr$ at 300°C and GHSV 4500 h^{-1}; ■ = conversion, ○ = selectivity to CO_x, □ = selectivity to acetic acid.

6.4.3 Effects of steam

Since water is involved in production of acetic acid from ethylene, the effect of steam flow on ethylene oxidation over $Nb_xPMo_{12}Pyr$ (x = 0.2, 0.6) at constant GHSV of 4500 h^{-1} and 300°C is shown by the data in Table 6.13. Trends for both Nb/P = 0.2 and 0.6 are similar but Nb/P = 0.6 yields a more active catalyst. At Nb/P = 0.6, carbon and oxygen conversion rise from 11 and 50% to 21 and 83%, respectively, as steam flow is increased from 8% to 50% of the total flow. Selectivity to acetic acid is maximized at 0.19 mmol/min/g_{cat} when the feed is composed of 50% steam. Selectivity and production of acrylic acid pass through a minimum at 33% steam while selectivity to maleic acid is relatively constant at 1%. The amount of carbon oxides decreases with increased steam. In the case of Nb/P = 0.6, the contribution of both CO and CO_2 to the product distribution decreases with increased steam feed. The catalysts are able to support up to 50% steam feed while increasing the production of acetic acid. The increase in acetic acid production is greatly enhanced for the case of Nb/P = 0.6, indicating that niobium may stabilize the catalyst towards water adsorption or desorption.

Nb/P	**Steam**	**Conversion (%)**		**Selectivity (%)**					**STY**		
		C_2H_4	**O2**	**CO**	**CO_x**	**AcA**	**Acr A**	**MA**	**AcA**	**Acr A**	**MA**
0.2	5	8	36	51	70	22	7.4	0.8	0.040	0.009	0.001
	10	11	45	43	61	33	5.6	1.0	0.077	0.009	0.001
	20	15	65	47	63	32	3.8	0.9	0.109	0.009	0.002
	30	14	60	38	55	37	7.1	1.4	0.111	0.014	0.002
0.6	5	11	50	49	68	36	4.7	1.0	0.068	0.008	0.001
	10	14	60	45	63	32	3.9	1.0	0.105	0.009	0.002
	20	15	61	40	54	42	2.6	1.3	0.146	0.006	0.002
	30	21	83	42	57	38	3.3	1.0	0.190	0.011	0.003

Table 6.13: Effect of steam flow on ethylene oxidation at GHSV 4500 h^{-1} and 300°C (total flow = 60 mL/min). Acr A = acrylic acid, MA = maleic acid, STY = space time yield (mmol/min/g_{cat}).

6.5 Results of ethanol oxidation

The selective oxidation of ethane to ethylene and acetic acid is believed to occur through an adsorbed ethoxy intermediate.[10,11] However, ethanol is observed in only trace amounts during ethane oxidation and not at all during ethylene oxidation over $Nb_{0.4}PMo_{12}Pyr$ at 240°C, most likely due to its high reactivity.

6.5.1 Effect of temperature

Ethanol may be easily dehydrated to form ethylene and ether, dehydrogenated to form ethyl acetate, partially oxidized to form acetaldehyde and acetic acid, or fully oxidized to carbon oxides. The ability of the heteropolyanion system to catalyze these reactions is probed by variations in temperature from 200 to 340°C. Results are shown in Table 6.14.

At 200 and 240°C dehydration reactions dominate as evidenced by the extremely low ethanol and oxygen conversions and the lack of significant amounts of acetic acid. Ethylene and ether are the major products. A dramatic shift in reaction profile occurs at 300°C where selectivity to acetic acid jumps from 1 to 14%, ethanol conversion jumps from 32 to 100%, and oxygen conversion jumps from 9 to 71%. Space time yield to acetic acid jumps two orders of magnitude from 0.007 to 0.30 mmol/min/g_{cat}. Ether production is eliminated, ethyl acetate production is decreased, and carbon oxide selectivity increases from 4 to 9%.

Raising the temperature to 340°C completely eliminates acetaldehyde and ethyl acetate production. Both ethanol and oxygen conversion are 100%. Carbon oxides remain low, comprising only 17% of the product profile. Ethylene space time yield drops slightly from 1.62 to 1.56 mmol/min/g_{cat} due to the increased carbon oxides. Acetic acid production remains high, reaching 0.34 mmol/min/g_{cat}. Thus, ethanol oxidation is activated at 300°C under hydrocarbon rich conditions and, unlike ethylene oxidation, is very selective to the partially oxidized products ethylene and acetic acid. Ethylene is the preferred product of ethanol oxidation.

T	**Conversion (%)**		**Selectivity (%)**								**STY**	
(^{o}C)	**EtOH**	**O_2**	**CO_x**	**C_2H_4**	**AcA**	**AcAl**	**Ether**	**EtAc**	**Acr A**	**MA**	**C_2H_4**	**AcA**
340	100	99	17	68	15	-	-	-	0.3	0.5	1.56	0.341
300	100	71	9	75	14	1	-	1	0.4	0.2	1.62	0.303
240	32	9	4	50	1	13	23	6	0.2	-	0.33	0.007
200	7	0	0	26	2	12	60	-	-	-	0.04	0.004

Table 6.14: Ethanol oxidation over $Nb_{0.6}PMo_{12}Pyr$ at GHSV 4500 h^{-1}. AcAl = acetaldehyde, EtAc = ethyl acetate, Acr A = acrylic acid, MA = maleic acid, STY = space time yield (mmol/min/g_{cat}).

Aside from increasing temperature, dehydration and dehydrogenation products can also be eliminated by limiting the amount of ethanol in the feed while under oxygen rich conditions. When ethanol is reduced from 16 mL/min to only 1mL/min under constant oxygen flow and total space velocity only carbon oxides, ethylene, and acetic acid are produced between 200 and 340^{o}C.

6.5.2 Effect of catalyst composition

The effect of framework and charge compensating ions on ethanol oxidation was studied to further understand the characteristics of the heteropolyanion system. Results are shown in Table 6.15. Both acid and cation exchanged forms of the catalysts show very high activity (greater than 70%) towards ethanol with ethylene as the major reaction product. However, addition of niobium in the acid form of the catalysts or within a cation exchanged catalyst increases conversion to nearly 100%. Additionally, only when niobium is present is oxidation to acetic acid appreciable. Furthermore, unselective partial oxidation and dehydration products are reduced with the addition of niobum. This indicates that niobium must be aiding in the efficient oxidation process of the catalysts. Contrary to the results of ethane and ethylene oxidation, even the acid form of the catalyst $PMo_{11}NbPyr$ is capable of selective oxidation and high conversion. In fact, space time yield to acetic acid for the acid form, 0.36 mmol/min/g_{cat}, is greater than for any other form of the catalyst examined.

Without the presence of niobium, the data given in Table 6.15 indicate that addition of vanadium to the catalyst decreases ethanol conversion and greatly enhances acetaldehyde and ether production at the expense of ethylene. When niobium and vanadium are both present, as in $Nb_{0.68}PMo_{11}VPyr$, acetic acid production is depressed (0.19 mmol/min/g_{cat}) as compared to either the acid form $PMo_{11}NbPyr$ (0.36 mmol/min/g_{cat}) or $Nb_{0.6}PMo_{12}Pyr$ (0.303 mmol/min/g_{cat}). Oxygen conversion is decreased from 71 to 38% as compared to $Nb_{0.6}PMo_{12}Pyr$ and acetaldehyde production is increased to from 1 to 6.2%. Thus, similar to ethane oxidation, the presence of vanadium is inhibitory to activity and selectivity.

Catalyst	Conversion (%)		Selectivity (%)						STY	
	EtOH	O_2	CO_x	C_2H_4	AcA	AcAl	Ether	EtAC	C_2H_4	AcA
$PMo_{12}Pyr$	100	9	1.2	89	1.2	9.2	-	-	2.06	0.028
$PMo_{11}VPyr$	73	16	1.9	52	2.5	23.7	17.0	2.6	0.89	0.042
$PMo_{11}NbPyr$	96	65	5.3	68	15.7	4.5	2.1	4.3	1.56	0.355
$Mo_{0.68}PMo_{12}Pyr$	98	9	0.9	88	1.4	8.1	1.1	0.1	1.88	0.029
$(VO)_{0.68}PMo_{12}Pyr$	86	11	0.3	67	2.2	20.1	8.9	1.3	1.15	0.038
$Nb_{0.68}PMo_{11}VPyr$	96	38	4.1	78	9.2	6.2	0.7	1.3	1.61	0.188
$Nb_{0.6}PMo_{12}Pyr$	100	71	8.9	75	14.1	1.0	-	1.1	1.62	0.303

Table 6.15: Ethanol oxidation as a function of catalyst composition at GHSV 4500 h^{-1} and 300°C. AcAl = acetaldehyde, EtAc = ethyl acetate, Acr A = acrylic acid, MA = maleic acid, STY = space time yield (mmol/min/g_{cat}).

6.6 References

(1) Holles, J. H.; Dillon, C. J.; Labinger, J. A.; Davis, M. E. *Journal of Catalysis* **2003**, *218*, 42-53.

(2) Wight, A., Ph.D. Thesis, California Institute of Technology, 2004.

(3) Tsigdinos, G. A.; Hallada, C. J. *Inorganic Chemistry* **1968**, *7*, 437-441.

(4) Min, J.-S.; Mizuno, N. *Catalysis Today* **2001**, *66*, 47-52.

(5) Albonetti, S.; Cavani, F.; Trifiro, F. *Catalysis Letters* **1995**, *30*, 253-262.

(6) Min, J.-S.; Misono, M.; Taguchi, A.; Mizuno, N. *Chemistry Letters* **2001**, *31*, 28-29.

(7) Fournier, M.; Feumi-Jantou, C.; Rabia, C.; Herve, G.; Launay, S. *Journal of Materials Chemistry* **1992**, *2*, 971-978.

(8) Ghizdavu, L.; Fodor, A.; Szasz, G. S. *Journal of Thermal Analysis and Calorimetry* **2001**, *63*, 907-9012.

(9) Dillon, C. J.; Holles, J. H.; Davis, R. J.; Labinger, J. A.; Davis, M. E. *Journal of Catalysis* **2003**, *218*, 54-66.

(10) Ruth, K.; Burch, R.; Kieffer, R. *Journal of Catalysis* **1998**, *175*, 27-39.

(11) Merzouki, M.; Taouk, B.; Monceaux, L.; Bordes, E.; Courtine, P. Studies in Surface Science and Catalysis, 1992; p 165-179.

(12) Linke, D.; Wolf, D.; Baerns, M.; Zeyβ, S.; Dingerdissen, U. *Journal of Catalysis* **2002**, *205*, 32-43.

(13) Linke, D.; Wolf, D.; Baerns, M.; Timpe, O.; Schlogl, R.; Zeyβ, S.; Dingerdissen, U. *Journal of Catalysis* **2002**, *205*, 16-31.

(14) Roy, M.; Ponceblanc, H.; Volta, J. C. *Topics in Catalysis* **2000**, *11/12*, 101-109.

(15) Tessier, L.; Bordes, E.; Gubelmann-Bonneau, M. *Catalysis Today* **1995**, *24*, 335-340.

(16) Davis, M. E.; Dillon, C. J.; Holles, J. H.; Labinger, J. *Angewandte Chemie International Edition* **2002**, *41*, 858-860.

(17) Marchal-Roch, C.; Millet, J.-M. M. *Comptes Rendus de l'Académie des Sciences - Series IIC - Chemistry* **2001**, *4*, 321-329.

(18) Song, I. K.; Barteau, M. A. *Langmuir* **2004**, *20*, 1850-1855.

(19) Kaba, M. S.; Song, I. K.; Barteau, M. A. *The Journal of Vacuum Science and Technology A, Vacuum, surfaces, and films* **1997**, *15*, 1299-1304.

(20) Song, I. K.; Barteau, M. A. *Journal of Molecular Catalysis A: Chemical* **2004**, *212*, 229-236.

(21) Min, J.-S.; Mizuno, N. *Catalysis Today* **2001**, *71*, 89-96.

(22) Mizuno, N.; Min, J.-S.; Taguchi, A. *Chemistry of Materials* **2004**, *16*, 2819-2825.

(23) Davies, T.; Taylor, S. H. *Catalysis Letters* **2004**, *93*, 151-154.

(24) Takehira, K.; Ohishi, Y.; Shishido, T.; Kawabata, T.; Takaki, K.; Zhang, Q.; Wang, Y. *Journal of Catalysis* **2004**, *224*, 404-416.

(25) Takahara, I.; Saito, M.; Inaba, M.; Murata, K. *Catalysis Letters* **2004**, *96*, 29-32.

(26) Dimitratos, N.; Vedrine, J. C. *Applied Catalysis A: General* **2003**, *256*, 251-263.

(27) Langpape, M.; Millet, J.-M. M. *Applied Catalysis A: General* **2000**, *200*, 89-101.

(28) Bhasin, M. M. *Topics in Catalysis* **2003**, *23*, 145-149.

(29) Ogasawara, K.; Iizuka, T.; Tanabe, K. *Chemistry Letters* **1984**, *15*, 645-648.

(30) Ruth, K.; Kieffer, R.; Burch, R. *Journal of Catalysis* **1998**, *175*, 16-26.

(31) Botella, P.; Nieto, J. M. L.; Solsona, B.; Mifsud, A.; Marquez, F. *Journal of Catalysis* **2002**, *209*, 445-455.